The Astrophysical Journal, 652:249–256, 2006 November 20

EVOLUTION OF THE GALAXY LUMINOSITY FUNCTION FOR REDSHIFT AND DENSITY ENVIRONMENT AT $0.03 < z < 0.5$

Lifang Xia,[1,2] Xu Zhou,[1] Yanbin Yang,[1] Jun Ma,[1] and Zhaoji Jiang[1]
Received 2006 April 10; accepted 2006 July 10

ABSTRACT

Using the galaxy sample observed by the Beijing-Arizona-Taiwan-Connecticut (BATC) large-field multicolor sky survey and the galaxy data of the Sloan Digital Sky Survey (SDSS) in overlapping fields, we study the dependence of the rest-frame *r*-band galaxy luminosity function on redshift and on the large-scale environment. The large-scale environment is defined by isodensity contours with density contrast $\delta\rho/\rho$. The data set is a composite sample of 69,671 galaxies with redshifts $0.03 < z < 0.5$ and $r < 21.5$ mag. The redshift data are composed of three parts: (1) spectroscopic redshifts in SDSS for local and the most luminous galaxies, (2) 20-color photometric redshifts derived from BATC and SDSS, and (3) five-color photometric redshifts in SDSS. We find that the faint-end slope α steepens slightly from -1.21 at $z \sim 0.06$ to -1.35 at $z \sim 0.4$, which is the natural consequence of the hierarchical formation of galaxies. The luminosity function also differs with different environments. The value of α changes from -1.21 in underdense regions to -1.37 in overdense regions, and the corresponding M_* brightens from -22.26 to -22.64. This suggests that the fraction of faint galaxies is larger in high-density regions than in low-density regions.

Subject headings: cosmology: observations — galaxies: distances and redshifts — galaxies: evolution — galaxies: luminosity function, mass function — large-scale structure of universe

1. INTRODUCTION

The galaxy luminosity function (LF) is a powerful tool in the study of galaxy formation and evolution. The galaxy LF is directly related to the galaxy mass function. Press & Schechter (1974) present a simple analytical formula for the mass distribution based on the hierarchical assembly of galaxies. Schechter (1976) gives an empirical functional form for the galaxy LF. It has been proposed that it should be universal (Lugger 1986; Colless 1989; Trentham 1998). However, the mass function, star formation process, and morphological characteristics of galaxies are affected by their environments and evolve with time, and so the galaxy LF is expected to change with time and to vary with galaxy characteristics and density environments. Deep wide-area sky surveys, such as the Two Degree Field Galaxy Redshift Survey (2dFGRS; Colless et al. 2001; Norberg et al. 2002) and the Sloan Digital Sky Survey (SDSS; York et al. 2000), can generate large samples with a range of redshifts, which are best suited for the measurement of the LF of galaxies. Many studies have been made of the galaxy LF, by morphological types (Wolf et al. 2003; Cross et al. 2004; Croton et al. 2005), by redshifts (Lilly et al. 1995; Ellis et al. 1996; Wolf et al. 2003; Loveday 2004), and by large-scale environments (Mercurio et al. 2003; Haines et al. 2004; Croton et al. 2005; Hoyle et al. 2005). These enable us to test theories of the formation and evolution of galaxies in different cosmological models.

Ellis et al. (1996) indicate that there is indeed a steepening in the faint-end slope with redshift. Since they were limited by the size of their data sets, however, the evolution of the LF to high redshift was not well constrained. For the galaxy LF of the large-scale environment, analyses reveal that, in a low-density environment (Efstathiou et al. 1988; Loveday et al. 1992; Hoyle et al. 2005), the faint-end slope turns out to be $\alpha \sim -1$, and in high-density regions the slope seems to be steeper, with $-1.8 < \alpha < -1.3$ (De Propris et al. 1995; Lumsden et al. 1997; Valotto et al. 1997).

In this paper, we use our BATC (Beijing-Arizona-Taiwan-Connecticut) 15 intermediate-band color sky survey data and SDSS five-color sky survey data to study the evolution of the LF and the environmental effects on the LF. The BATC photometric system has an average depth of 20.5 mag, and the corresponding redshifts of most galaxies are less than 0.3. The SDSS broadband photometric system has an average depth of 23.0 mag, with most redshifts less than 0.5. From the investigation in Xia et al. (2002), the accuracy of redshift determination by 15 intermediate bands, $\sigma_z \sim 0.02$, is much better than that of the broadband, $\sigma_z \sim 0.05$, with the same photometric magnitude errors. Therefore, with accurate photometric redshifts at $z < 0.3$ and with small values of $\Delta z/z$ at $0.3 < z < 0.5$, it is possible to combine the data of these two photometric systems for accurate measurements of the galaxy LF to high redshifts.

The content of this paper is as follows. In § 2 we briefly describe the data sample, the application of the photometric redshift code `hyperz`, and *k*-correction. The fitting of the galaxy LF and results of the LF evolution are given in § 3. The method of environmental classification and the results of environmental effects on the LF are presented in § 4. Section 5 discusses the effects of photometric redshift uncertainty on the galaxy LF shape by simulation and summarizes our conclusions. Throughout this paper, we assume a ΛCDM cosmological model with matter density $\Omega_m = 0.3$, vacuum density $\Omega_\Lambda = 0.7$, and Hubble constant $H_0 = 100\ h$ km s^{-1} Mpc^{-1}, with $h = 0.75$ for the calculation of distances and volumes (see Hogg 1999).

2. DATA

2.1. *Sample*

We use galaxy data including BATC 15-color photometries and SDSS spectroscopies and five-color photometries. The BATC sky survey performs photometric observations with a large-field

[1] National Astronomical Observatories, Chinese Academy of Sciences, Beijing, 100012, China; xlf@vega.bac.pku.edu.cn, zhouxu@vega.bac.pku.edu.cn.
[2] Department of Astronomy, Peking University, Beijing, 100871, China.

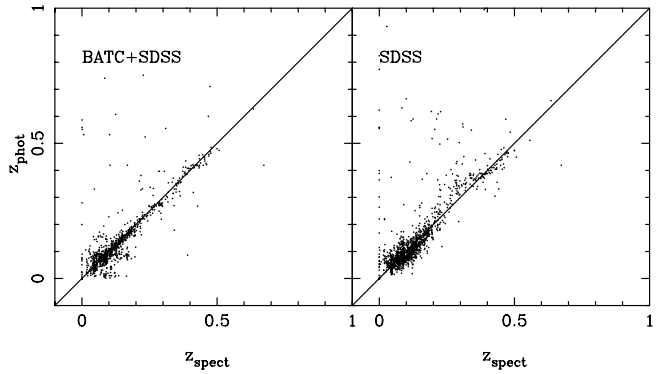

FIG. 1.—Comparison between photometric and spectroscopic redshifts, estimated by 20 colors of BATC and SDSS (*left*) and 5 colors of SDSS (*right*), respectively.

multicolor system. The observations are carried out with the 60/90 cm f/3 Schmidt Telescope of the National Astronomical Observatories, Chinese Academy of Sciences (NAOC), located at the Xinglong station. For a detailed description of the survey and performance, see Zhou et al. (2001). The SDSS performs imaging and spectroscopic surveys over π steradians in the northern Galactic cap with a 2.5 m telescope at Apache Point Observatory, Sunspot, New Mexico (York et al. 2000). A detailed description of the photometric and spectroscopic parameters can be found in Stoughton et al. (2002).

We select 17 fields, totaling $\sim$17 deg^2, observed by BATC that overlap with the SDSS sky survey. Galaxies with the spectroscopic and photometric information in SDSS are obtained from SDSS Data Release 2.[3] The data of 69,671 galaxies with $r < 21.5$ and $0.03 < z < 0.5$ are compiled in the SDSS. Galaxies in BATC are selected by coordinates given by BATC and SDSS, and 10,681 galaxies in BATC are obtained, with distance deviations in BATC and SDSS of less than 2.″0. To combine photometries in BATC and SDSS, we need to apply an aperture correction to the SDSS model magnitudes, since an aperture of 4 pixels (i.e., $r_{ap} = 6.''8$) is applied to BATC photometries (see details from Yuan et al. 2003). The formula used for the aperture correction is

$$\Delta m = m_{ap} - m_{model} = -2.5 \log \frac{\int_0^{r_{ap}} 2\pi r I(r)\, dr}{\int_0^{\infty} 2\pi r I(r)\, dr}, \qquad (1)$$

where m_{ap} is the aperture magnitude and $I(r)$ is the profile function of the surface intensity for the best fit of a de Vaucouleurs or exponential model. For these common galaxies, we estimate photometric redshifts using all 20 colors.

2.2. *Redshift*

The redshifts in our catalog are measured by three methods. Of our galaxies, 1362 have spectroscopic redshifts observed by SDSS, 10,681 have photometric redshifts estimated by 20-color photometries from BATC and SDSS, and the remaining 57,628 have photometric redshifts estimated by five-color photometries from the SDSS. The photometric redshift technique is based on spectral energy distribution (SED) fitting to estimate redshifts by comparing the spectrum of an object, which should include several strong spectral features such as the 4000 Å break and the Lyman forest decrement, with the template spectra. We use the `hyperz` program developed by Bolzonella et al. (2000) to estimate redshifts. The accuracy of redshift determination in BATC has reached 0.02, and the estimated accuracy by broadband filters is about 0.05 (Xia et al. 2002).

[3] See http://www.sdss.org/dr2.

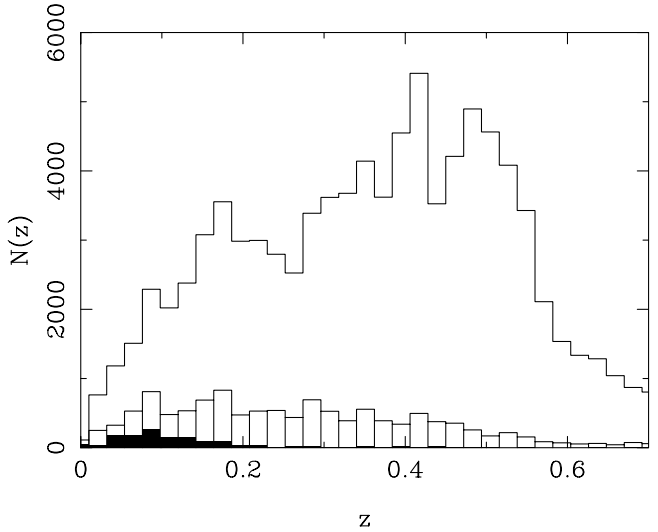

FIG. 2.—Redshift distributions for total galaxies (*open histogram*), galaxies with 20-color photometric redshifts (*bar histogram*), and galaxies with spectroscopic redshifts (*filled histogram*).

The accuracy of photometric redshifts is assessed by comparing galaxies with spectroscopic redshifts in the fields for both systems. Figure 1 shows a comparison between photometric redshifts and spectroscopic redshifts. We can distinctly see that redshifts of some galaxies are overestimated by the five-color SDSS photometries. The combined 20 colors can bring them back to a reasonable estimation. The redshifts in the range 0.3–0.4 seem to be overestimated in the SDSS; this may dramatically affect the measure of the LF because of the preponderance of galaxies from the SDSS in high-redshift layers. The uncertainties are $\sigma = 0.017$ for 20-color galaxies and $\sigma = 0.022$ for five-color galaxies, excluding those with $\Delta z > 0.05$. Given that the galaxies used to estimate accuracy are bright in magnitude and accurate in photometry, for faint galaxies, the errors of estimated photometric redshifts should be larger than these estimates. To assess how the uncertainty of the photometric redshift affects the predicted LF, we investigate using a simulation in § 5. Galaxies with $z < 0.03$ are excluded in the construction of galaxy luminosity for the large relative errors for local galaxies. Figure 2 shows the distribution of galaxy redshifts in our composite sample. The first histogram, indicated with a simple line, shows the redshift distribution for the total galaxy sample. The second histogram shows the distribution for galaxies with 20 colors. The third histogram, indicated with the filled area, shows the distribution for galaxies with spectroscopic redshifts. Figure 2 shows us directly the contributions from these three sources.

2.3. *The k-Correction*

Using photometric redshifts, we calculate the absolute magnitudes in the rest-frame r band of SDSS:

$$M_r = r - 25 - 5 \log d_L(z) - A_r - k(z), \qquad (2)$$

where $d_L(z)$ is the luminosity distance in units of Mpc, A_r is the reddening extinction correction due to intergalactic and interstellar dust scattering and absorption, and $k(z)$ is the k-correction due to the shift of the spectrum by redshift. Here the k-correction is significant, since the sampled redshifts span to high redshifts.

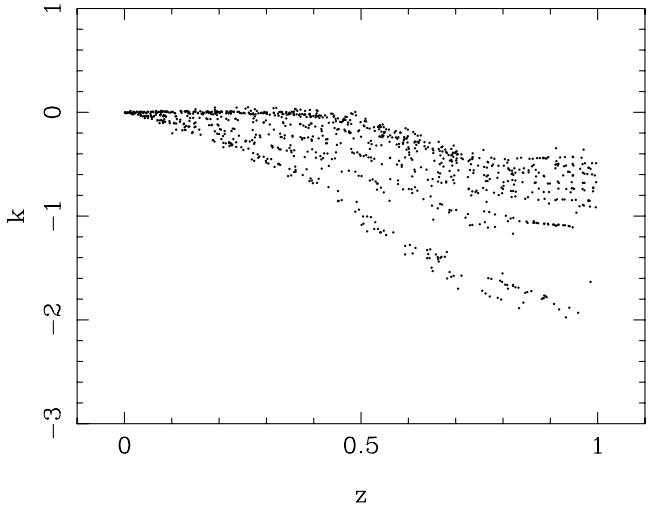

FIG. 3.—Distribution of simulated *k*-correction with redshift.

The commonly applied method is to estimate the *k*-correction by galaxy color and morphological type. The advantage of photometric redshift fitting is that we can derive *k*-corrections directly from the spectra templates. In photometric redshift fitting, a best-fit template can be achieved for every galaxy, which is the one that most resembles the spectrum shape. We slightly modify the code and output the best-fit template spectrum at $z = 0$. If we assume that the observed spectrum has the same *k*-correction as the best-fit template, the *k*-correction can be made directly. We investigate the accuracy of this correction here by using a simulation.

Using the procedure `makecatalog` (see details in Xia et al. 2002), we build a catalog of 1000 galaxies with random types from Bruzual & Charlot (1993) and redshifts in the range of $z < 0.5$. In total, 20 filters are used. The model *k*-corrections are output directly from `makecatalog`, and the estimated corrections are output by `hyperz`. Hence, we can estimate the accuracy of the *k*-correction. Figure 3 shows the distribution of the corrections with redshifts. The corrections $k(z)$ in the rest-frame *r* band range from 0 to 2 mag. Figure 4 shows the comparison between model and estimated corrections and the distribution of the deviations. The rms error of the *k*-correction is about 0.05 mag, with a small offset of 0.01 mag.

Reddening extinction is obtained by step fitting in `hyperz` (Xia et al. 2002). We adopt the reddening law of Allen (1976, p. 264) for the Milky Way. The value of the reddening correction is that best fitted by the template spectrum. Here we also assess the accuracy of the total correction of the reddening extinction A_r and the *k*-correction by using a simulation. We find that the rms error of this total correction is about 0.08 mag, with a small offset of 0.01 mag. In § 5 we demonstrate with a simulation that the magnitude error plays the most important role in the prediction of the LF and that this magnitude error will affect the LF fit slightly.

3. EVOLUTION OF LUMINOSITY FUNCTION

The luminosity function is the number density of galaxies as a function of luminosity. To measure the LF, we adopt the approximation of the Schechter function (Schechter 1976),

$$\Phi(L)\,dL = \phi_*\left(\frac{L}{L_*}\right)^{\alpha}\exp\left(-\frac{L}{L_*}\right)d\left(\frac{L}{L_*}\right), \qquad (3)$$

expressed per unit absolute magnitude:

$$\Phi(M)\,dM = 0.4\ln(10)\phi_* 10^{-0.4(M-M_*)(\alpha+1)} \times \exp\left(-10^{-0.4(M-M_*)}\right)dM, \qquad (4)$$

where M_* is the characteristic magnitude, i.e., the point at which the bright-end cutoff sets in, corresponding to L_*, α is the power-law slope of the faint end, and ϕ_* is the normalization constant. We search these parameters by χ^2 minimization fitting. The fits are performed over the magnitude range $-24 < M_i < -16$, and the normalizations are also done in this magnitude range.

To correct the incompleteness arising from the selection effects of distance, the traditional $1/V(M)$ method originally proposed by Schmidt (1968) is implemented in this paper. With the assumption that galaxies are distributed homogeneously in comoving space, the correction function is $1/V(M)$, where $V(M)$ is the maximum volume determined by the maximum distance at which a galaxy with absolute magnitude M can be observed in the

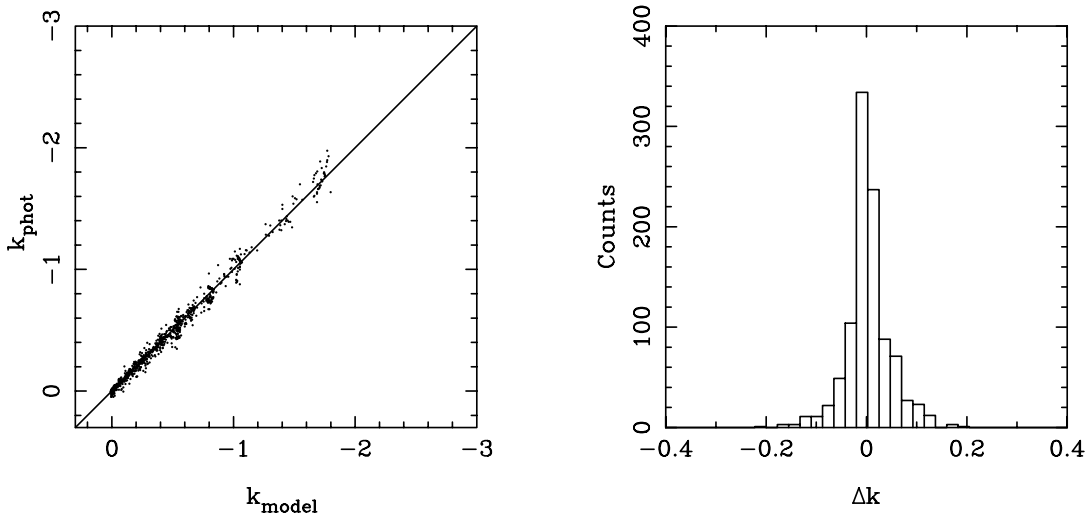

FIG. 4.—Assessment of the accuracy of the *k*-correction and the reddening extinction. The left panel shows a comparison between the model correction and the estimated correction. The right panel shows the distribution of the deviations.

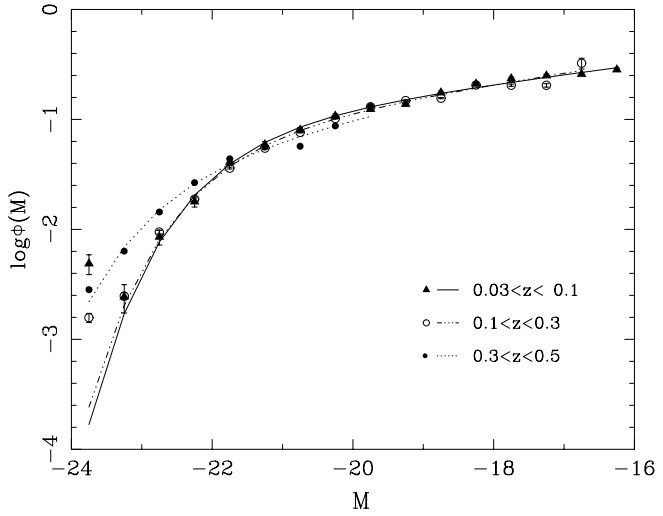

FIG. 5.—Luminosity functions fitted for the three redshift layers $0.03 < z < 0.1$ (*filled triangles, solid line*), $0.1 < z < 0.3$ (*open circles, triple-dot–dashed line*), and $0.3 < z < 0.5$ (*filled circles, dotted line*).

apparent magnitude limit. The comoving volume and luminosity distance are calculated as given by Hogg (1999):

$$dV_C = \frac{c}{H_0}\frac{d_L(z)^2}{(1+z)^2 E(z)}\,d\Omega\,dz, \tag{5}$$

$$d_L(z) = (1+z)\frac{c}{H_0}\int_0^z \frac{dz'}{E(z')},$$

$$E(z) = \sqrt{\Omega_m(1+z)^3 + \Omega_\Lambda}. \tag{6}$$

Small-scale structure and the possible evolution in number density with redshift can produce a spurious estimate of the local LF in this formulation. However, the large size of the data set may partly make up for the effect caused by inhomogeneity. The Malmquist bias in distance estimates originates from the observational effect that there are greater numbers of galaxies in the universe at greater distances, and hence more will have been scattered down from larger distances than up from smaller ones. We follow the method given by Lynden-Bell et al. (1988) to correct the distance estimates. The correction formula is

$$R = R_e \exp\left[\left(\alpha + \frac{1}{2}\right)\Delta^2\right], \tag{7}$$

where R_e is the estimated luminosity distance D_L, $\alpha = 3$ for uniform distribution, and Δ is the dispersion in $\ln R_e$.

To study the evolution of the galaxy LF, we split our galaxy sample into three redshift layers, $0.03 < z < 0.1$, $0.1 < z < 0.3$, and $0.3 < z < 0.5$, with 5289, 26,162, and 38,220 galaxies, respectively. Figure 5 shows the LFs derived for the three layers $0.03 < z < 0.1$ (*filled triangles, solid line*), $0.1 < z < 0.3$ (*open circles, triple-dot–dashed line*), and $0.3 < z < 0.5$ (*filled circles, dotted line*). The error bars are the errors of Poisson counts. Measured parameters are given in Table 1, and the error contours are plotted in the left panel of Figure 6. As shown in Figure 5 and Table 1, the faint-end slope α steepens slightly from -1.21 ± 0.02 to -1.25 ± 0.03 and -1.35 ± 0.08 with the increase of redshift. The points appear to show some discrepancy with the Schechter function at the bright end. The first point is higher, which might be for several reasons. First, it may be due to observational effects. For the nearest galaxies, uncertain proper motions can lead to large errors in redshift and hence to overestimation of the most luminous galaxies. On the other hand, the number of intermediate luminous galaxies is much greater than the number of the most luminous galaxies in the observation, so the uncertainty of magnitude and photometric redshift can shift more intermediate-redshift galaxies to low redshifts, contributing to the excess of the most luminous galaxies.

For local galaxies in the range $0.03 < z < 0.1$, the value of $\alpha = -1.21 \pm 0.02$ is consistent with that of Blanton et al. (2001), $\alpha = -1.20 \pm 0.03$, which was achieved by using 11,275 galaxies that were complete to $r < 17.6$ over 140 deg^2 in the SDSS. Blanton et al. (2003) reevaluated the galaxy LF at $z = 0.1$ in the $^{0.1}r$ frame using a larger sample of 147,986 galaxies. A much flatter faint-end slope of $\alpha = -1.05 \pm 0.01$ was found. This large difference is due to the fact that Blanton et al. (2003) take the evolution of the LF into account.

From the redshift layer at $0.1 < z < 0.3$ to that at $0.3 < z < 0.5$, the estimated faint-end slope is found to change from $\alpha = -1.25 \pm 0.03$ to $\alpha = -1.35 \pm 0.08$. Ellis et al. (1996) constructed LFs using a sample of 1700 galaxies observed by the Autofib Redshift Survey out to $z \sim 0.75$ and found that the value of α steepens from -1.1 to -1.5 with redshift. Our results are in good agreement with this trend. Loveday (2004) studied the evolution of the LF at $z < 0.3$ using a sample of 162,989 spectroscopic galaxies with a magnitude limit of $r < 17.6$ in the SDSS. The poorly constrained faint-end slope in the redshift slice $0.2 < z < 0.3$ is due to the incompleteness in high redshift, with a bright magnitude limit of $r < 17.6$. Loveday (2004) investigated the effect of different absolute magnitude ranges on the estimated faint-end slope, and found that the faint-end slope α changes from -1.17 to -2.18 if the analysis of the redshift slice at $0.1 < z < 0.15$ is limited to $M_{0.1_r} < -21.5$. This effect will probably cause an overestimate of the faint-end slope for the redshift layer at $0.3 < z < 0.5$ in our sample: basically, there are no low-luminosity points to tie down the faint end. Although this is not obvious from the incompleteness of the redshift slice at $0.1 < z < 0.3$ in Figure 5, it could result from an incomplete sample as well.

TABLE 1
SHAPE PARAMETERS OF LFS

Subsample	Number of Galaxies	ϕ_* ($\times 10^{-2}$)	M_*	α_*	χ^2
$0.03 < z < 0.1$	5289	10.16 ± 0.08	-21.80 ± 0.16	-1.21 ± 0.02	0.43
$0.1 < z < 0.3$	26162	8.56 ± 0.13	-21.91 ± 0.12	-1.25 ± 0.03	2.59
$0.3 < z < 0.5$	38220	4.42 ± 0.17	-22.69 ± 0.21	-1.35 ± 0.08	29.77
High density	54267	4.14 ± 0.09	-22.64 ± 0.18	-1.37 ± 0.04	10.78
Low density	15404	8.83 ± 0.05	-22.26 ± 0.16	-1.21 ± 0.04	2.92

NOTE.—Shape parameters of LFs fitted to the three redshift-binned subsamples and those fitted to the high- and low-density subsamples, separated at density contrast $\delta\rho/\rho = 30$.

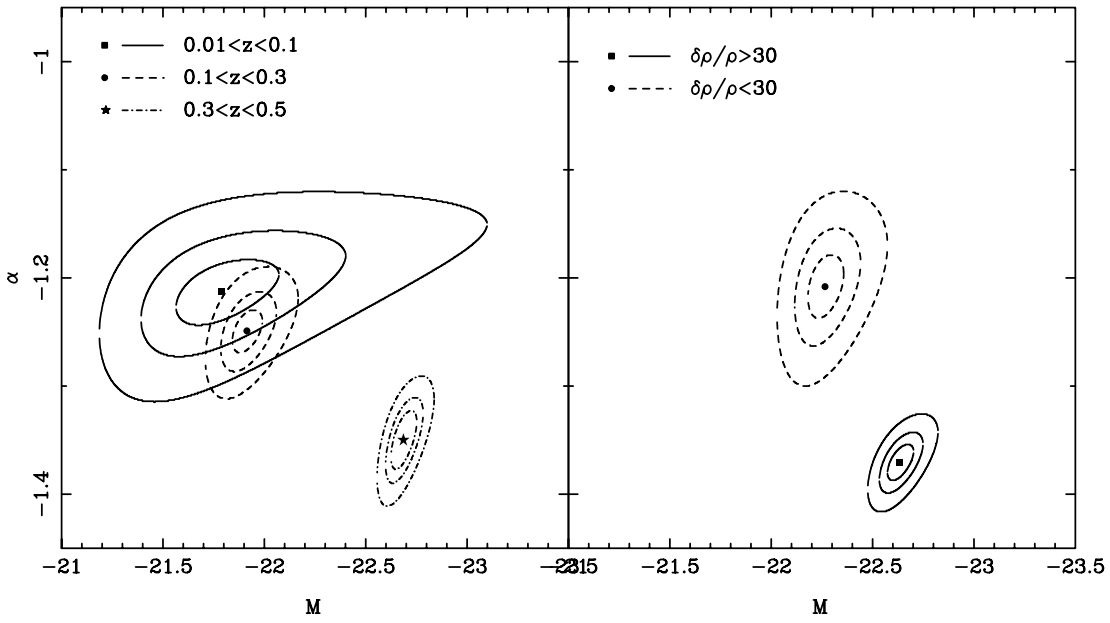

FIG. 6.—Error contours of 1 σ, 2 σ, and 3 σ for parameters M_* and α. The left panel shows them for the three redshift-layer $0.03 < z < 0.1$ (*solid lines*), $0.1 < z < 0.3$ (*dashed lines*), and $0.3 < z < 0.5$ (*dot-dashed lines*) subsamples. The right panel shows them for the overdense (*solid lines*) and underdense (*dashed lines*) subsamples.

The estimated characteristic magnitudes, which are $M_* = -21.80 \pm 0.16$, -21.91 ± 0.12, and -22.69 ± 0.21 for the three redshift layers, are ~1–2 mag brighter than previous results (Ellis et al. 1996; Blanton et al. 2001, 2003; Loveday 2004). This is partly due to a different choice of Hubble constant, using $h = 0.75$ when others have used $h = 1$. Another factor is the effect of larger magnitude errors and photometric redshift errors than from spectroscopic samples. We demonstrate this effect in § 5.

4. DEPENDENCE OF LUMINOSITY FUNCTION ON ENVIRONMENT

To study the dependence of the galaxy luminosity function on the large-scale density environment, we subdivide galaxies into two subsamples, high and low density, according to the density enhancements in three-dimensional redshift space. There are many methods implemented in the literature; here we use the percolation algorithm (Huchra & Geller 1982), which can search isolated groups and clusters. The algorithm identifies every pair of galaxies by the projected separation D_{12} and the line-of-sight redshift separation z_{12}:

$$D_{12} = \sin(\theta/2)(z_1 + z_2)c/H_0 < D_L(z_1, z_2, m_1, m_2), \quad (8)$$

$$z_{12} = |z_1 - z_2| < z_L(z_1, z_2, m_1, m_2), \quad (9)$$

where z_1 and z_2 refer to the redshifts of the two galaxies in the pair, θ is their angular separation, and D_L and z_L are scaled to account for the magnitude limit of the galaxy catalog. All pairs linked by a common galaxy form a group. The limiting number density contrast is

$$\frac{\delta\rho}{\rho} = \frac{3}{4\pi D_0^3}\left[\int_{-\infty}^{M_l} \Phi(M)\, dM\right]^{-1} - 1, \quad (10)$$

where $\Phi(M)$ is the luminosity function and M_l is the faintest absolute magnitude for galaxies with a magnitude limit at the fiducial distance. For a chosen density contrast and LF (assumed to be without evolution for simplicity), the critical distance D_0 can be calculated. When we take into account the decrease in the number of galaxies with increasing distance, the link parameter R can be calculated by

$$R = \left[\frac{\int_{-\infty}^{M_l} \Phi(M)\, dM}{\int_{-\infty}^{M_{12}} \Phi(M)\, dM}\right]^{1/3}. \quad (11)$$

In this expression, M_{12} is the faintest absolute magnitude for a galaxy with a magnitude limit at the mean distance of the two galaxies. Then $D_L = RD_0$ and $z_L = Rz_0$. The magnitude limit here is the complete magnitude. The fiducial redshift z_0 that we choose is the minimum redshift of the sample, $z_f = 0.03$, D_0 is the fiducial distance corresponding to z_f, and $\Phi(M)$ is chosen to be that measured by Blanton et al. (2001) for local galaxies,

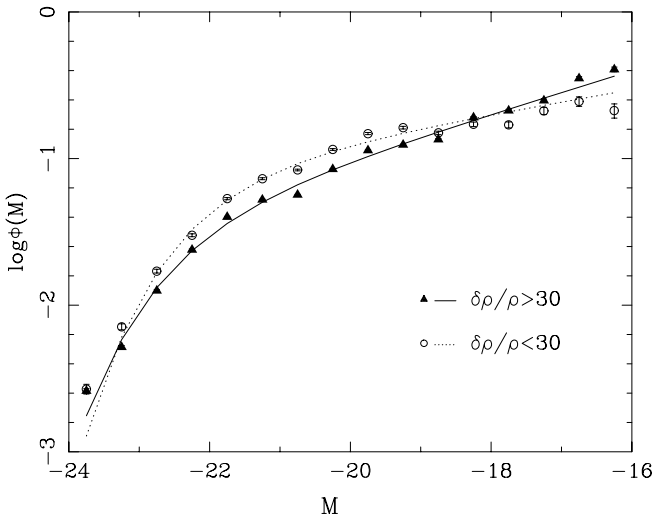

FIG. 7.—Luminosity functions fitted for the overdense and underdense subsamples.

TABLE 2
SIMULATED RESULTS OF THE ACCURACY OF LF PARAMETERS

σ_m	σ_z	$M_{*,\,\mathrm{fitted}}$	σ_{M_*}	$\alpha_{*,\,\mathrm{fitted}}$	σ_{α_*}
0.05.....	0.05	−21.28	0.076	−1.28	0.014
	0.20	−21.53	0.137	−1.19	0.017
	0.50	−21.38	0.123	−0.93	0.022
0.20.....	0.05	−21.28	0.071	−1.28	0.013
	0.20	−21.53	0.147	−1.21	0.028
	0.50	−21.38	0.120	−0.94	0.023
0.50.....	0.05	−21.28	0.065	−1.28	0.015
	0.20	−21.53	0.118	−1.18	0.017
	0.50	−21.48	0.117	−0.95	0.028

NOTES.—Simulated results of the accuracy of luminosity function parameters with different magnitude uncertainties and redshift uncertainties. The given parameters of the luminosity function are $M_* = -21.17$ and $\alpha_* = -1.26$.

using the SDSS commissioning data. The LF parameters are $\phi_* = 1.46 \times 10^{-2}\ h^3\ \mathrm{Mpc}^{-3}$, $M_* = -20.83$, and $\alpha = -1.20$. With these criteria, we can obtain our subsamples by using $\delta\rho/\rho$. We choose a value of $\delta\rho/\rho = 30$ for our classification, with the fiducial distance D_0 corresponding to about 0.35 Mpc. In this scale, the high-density subsample includes group galaxies and cluster galaxies (with five or more members) and the low-density subsample contains field and void galaxies. We obtain two subsamples containing 54,267 and 15,404 galaxies, respectively.

Figure 7 shows the luminosity functions derived for the subsamples classified by density environment. The discrepancy in fits may be due to the same reason given above. The best-fit Schechter parameters, along with the number of galaxies considered in each density environment, are listed in Table 1. From Table 1 we can see that, with increasing density, the faint-end slope rises from -1.21 ± 0.04 to -1.37 ± 0.04 and the characteristic magnitude brightens slightly from -22.26 ± 0.16 to -22.64 ± 0.18. The right panel of Figure 6 shows the 1 σ (68.3%; two parameters), 2 σ (95%; two parameters), and 3 σ χ^2 contours in the α-M_* plane for the high- and low-density populations. The difference is obviously significant at a confidence level of 95%. Since the curves in Figure 7 are normalized in the magnitude range $-24 < M_i < -16$, the bright-end density of underdense populations does not mean that the number of luminous galaxies is greater in underdense regions than in overdense regions.

Croton et al. (2005) examine the luminosity function by density environment. They use galaxies observed by 2dFGRS, with a median survey depth of $z \approx 0.11$. The local density contrast is determined by δ_8. The same tendency of α is given for regions with different density contrast. In numerical simulations, Mo et al. (2004) studied the dependence of the galaxy LF on the large-scale environment in hierarchical cosmology. Their results predict that the characteristic luminosity, L_*, increases moderately with density and that the faint-end slope is quite independent of density overall. The quantity α is virtually constant for late types and increases from -1.3 in underdense regions to -1.8 in overdense regions for early types. Although our samples are not split into subsamples by galaxy types, the predictions are broadly in good agreement. The steepening of the faint-end slope from underdense environments to overdense environments is explained in Tully et al. (2002) by a process of photoionization of the intergalactic medium that suppressed dwarf galaxy formation. Overdense regions typically collapse early and can form a dwarf galaxy before the epoch of reionization. Underdense regions, however, collapse later and are thus subject to the photoionization suppression of cooling baryons. The brightening of the characteristic magnitude in dense regions is consistent with the morphology-density relation (Dressler 1980; Binggeli et al. 1988), which indicates that the population in low-density subsamples is dominated by late types and that cluster regions have a relative excess of the most luminous early-type galaxies. In structure evolution models, it is proposed that the most dense regions of the universe will have collapsed earlier, have larger merger rates, and will contain more massive early-type galaxies.

5. DISCUSSION AND CONCLUSION

The uncertainties of galaxy photometric redshifts are ~0.01–0.4 in different photometric magnitude uncertainties. This is the best accuracy achieved by multicolor photometric information. This uncertainty, however, is much bigger than that of spectroscopic redshifts, which can be 0.0001. To calculate the luminosity function with photometric redshifts, we need to know how the

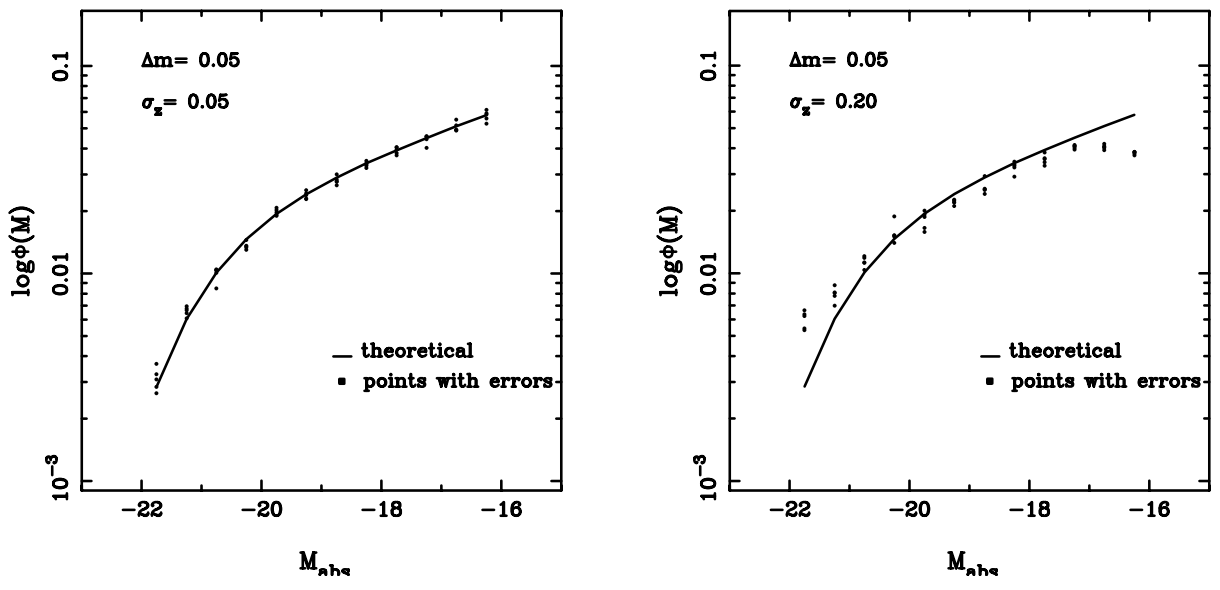

FIG. 8.—Luminosity function distribution of the 100 simulations with a Gaussian-distributed photometric uncertainty of 0.05 and redshift uncertainties of 0.05 and 0.20.

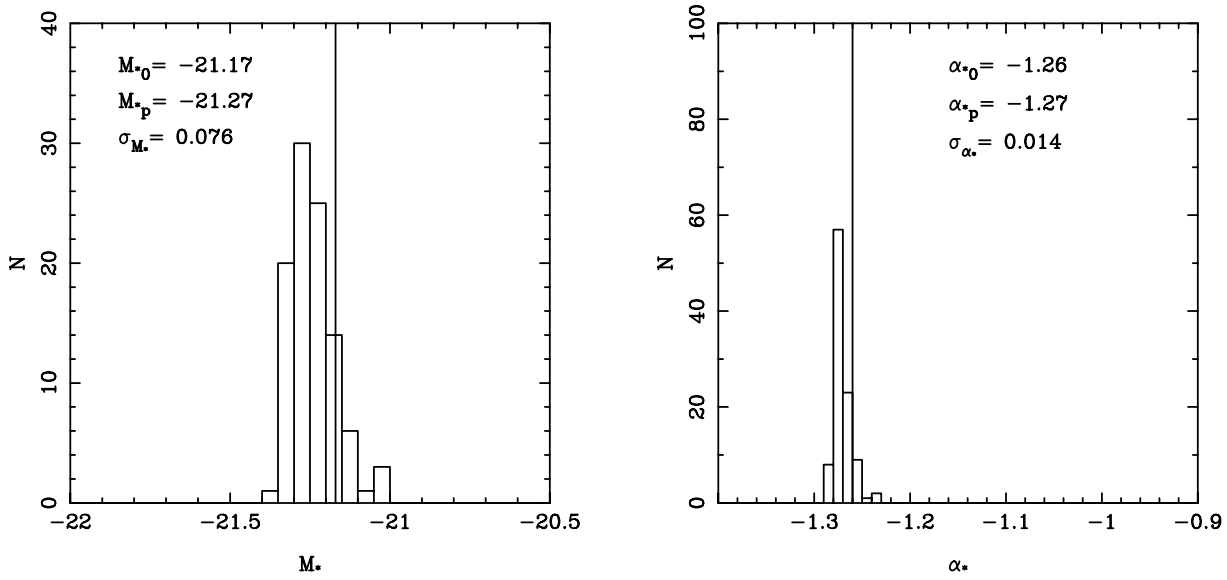

FIG. 9.—Distribution of fitted values of M_* and α for the simulated sample shown in the left panel of Fig. 8.

redshift uncertainty and photometric magnitude uncertainty affect the shape of the luminosity function. To assess this effect, we perform a series of simulations to fit the luminosity function for a galaxy sample distributed as a given luminosity function. We created 100 galaxy samples to evaluate the uncertainty of the fitted M_* and α. Each sample contains 5000 galaxies homogeneously distributed in the 1 deg^2 cone-shaped comoving space in the redshift range $z < 0.6$. Gaussian-distributed photometric errors with $\Delta m = 0.05$, 0.20, and 0.50 are assumed. We adopt a Gaussian distribution with a Gaussian kernel of width $\sigma_z = \hat{\sigma}_z(1+z)$ for photometric redshift errors, where $\hat{\sigma}_z$ is the redshift rms residual at zero redshift (Fernández-Soto et al. 2001; Chen et al. 2003). We assume values of $\hat{\sigma}_z = 0.05$, 0.20, and 0.50. Here we choose a given luminosity function with $M_* = -21.17$ and $\alpha = -1.26$.

Table 2 lists the estimated rms errors of M_* and α for different photometric uncertainties and redshift uncertainties. We find that the faint-end slope α becomes flatter and the characteristic magnitude M_* becomes brighter for all uncertainties. This means that the shapes of the luminosity function become flatter, which is demonstrated intuitively in Figure 8. Figure 8 shows the luminosity function distribution for Gaussian-distributed photometric uncertainties of 0.05 and redshift uncertainties of 0.05 and 0.20. Figure 9 shows the distribution of M_* and α in the 100 simulations with the same uncertainties as in the left panel of Figure 8. From Table 2, with the increase of redshift uncertainties, the characteristic magnitude M_* is determined with an offset of $\sim$0.2 mag brighter and an rms uncertainty of $\sim$0.1 mag, and α is determined with an offset of $\sim$0.2 flatter and an rms uncertainty of $\sim$0.02. The errors become larger with increasing photometric and redshift uncertainties. We can see from the simulation that photometric errors and redshift errors are two major factors in the measurement of the luminosity function. This change in the trends of M_* and α can partially explain the difference between our estimates and previous results.

We study the evolution of the galaxy luminosity function in the rest-frame r band and the dependence of the luminosity function on the density environment out to $z \sim 0.5$ by using 69,671 galaxies identified by the BATC sky survey and the SDSS. We increase the depth with photometric redshifts and adopt the Schechter function as our luminosity function model. The evolution of the galaxy luminosity function is studied with three redshift layers, $0.03 < z < 0.1$, $0.1 < z < 0.3$, and $0.3 < z < 0.5$. We subdivide the density environment using the criterion of an isodensity contour. The density contrast is chosen to be $\delta\rho/\rho = 30$. We summarize our principal conclusions as follows:

1. Through simulations, we find that the photometric uncertainty and the redshift uncertainty are two major factors that affect the measurement of the luminosity function. With a photometric uncertainty of $\Delta m < 0.50$ and a redshift uncertainty of $\hat{\sigma}_z < 0.50$, the characteristic magnitude, M_*, can be estimated to be 0.2 mag brighter, with a rms error of about $\sigma_{M_*} = 0.1$, and the faint-end slope, α, can be recovered as a factor of 0.2 flatter, with a small uncertainty of about $\sigma_\alpha = 0.02$.
2. There is slight evolution in the shape of the galaxy luminosity function with observational depth. We further the accurate measurement of the galaxy luminosity function to $z < 0.3$. The faint-end slope steepens slightly from -1.21 to -1.25 to -1.35 with the increase of redshift from $0.03 < z < 0.1$ to $0.1 < z < 0.3$ to $0.3 < z < 0.5$, respectively. The change in α is broadly consistent with previous claims, such as those of Lilly et al. (1995) and Ellis et al. (1996).
3. The luminosity function differs distinctly with the density environment. The faint-end slope for high-density galaxies is steeper than that for low-density galaxies. The value of α changes from -1.21 in underdense regions to -1.37 in high-density regions, and M_* brightens from -22.26 to -22.64.

We would like to thank the referee, Jon Loveday, for his insightful comments and suggestions that improved this paper significantly. We would like to acknowledge very helpful discussions with Zhenyu Wu, Jiuli Li, Zhonglue Wen, Tianmeng Zhang, Jianghua Wu, and Yuzhi Duan. We would also like to thank David Burstin and Zuhui Fan for their helpful revision of and suggestions regarding the paper. This work has been supported by the Chinese National Nature Science Foundation grants 10473012, 10573020, 10333060, and 10633020.

REFERENCES

Allen, C. W. 1976, Astrophysical Quantities (3rd ed.; London: Athlone Press)
Binggeli, B., Sandage, A., & Tammann, G. A. 1988, ARA&A, 26, 509
Blanton, M. R., et al. 2001, AJ, 121, 2358
———. 2003, ApJ, 592, 819
Bolzonella, M., Miralles, J.-M., & Pelló, R. 2000, A&A, 363, 476
Bruzual, A. G., & Charlot, S. 1993, ApJ, 405, 538
Chen, H.-W., et al. 2003, ApJ, 586, 745
Colless, M. 1989, MNRAS, 237, 799
Colless, M., et al. 2001, MNRAS, 328, 1039
Cross, N. J. G., et al. 2004, AJ, 128, 1990
Croton, D. J., et al. 2005, MNRAS, 356, 1155
De Propris, R., Pritchet, C. J., Harris, W. E., & McClure, R. D. 1995, ApJ, 450, 534
Dressler, A. 1980, ApJ, 236, 351
Efstathiou, G., Ellis, R. S., & Peterson, B. A. 1988, MNRAS, 232, 431
Ellis, R. S., Colless, M., Broadhurst, T., Heyl, J., & Glazebrook, K. 1996, MNRAS, 280, 235
Fernández-Soto, A., Lanzetta, K. M., Chen, H.-W., Pascarelle, S. M., & Yahata, N. 2001, ApJS, 135, 41
Haines, C. P., Mercurio, A., Merluzzi, P., La Barbera, F., Massarotti, M., Busarello, G., & Girardi, M. 2004, A&A, 425, 783
Hogg, D. W. 1999, preprint (astro-ph/9905116)
Hoyle, F., Rojas, R. R., Vogeley, M. S., & Brinkmann, J. 2005, ApJ, 620, 618
Huchra, J. P., & Geller, M. J. 1982, ApJ, 257, 423
Lilly, S. J., Tresse, L., Hammer, F., Crampton, D., & Le Fevre, O. 1995, ApJ, 455, 108
Loveday, J. 2004, MNRAS, 347, 601
Loveday, J., Peterson, B. A., Efstathiou, G., & Maddox, S. J. 1992, ApJ, 390, 338
Lugger, P. M. 1986, ApJ, 303, 535
Lumsden, S. L., Collins, C. A., Nichol, R. C., Eke, V. R., & Guzzo, L. 1997, MNRAS, 290, 119
Lynden-Bell, D., et al. 1988, ApJ, 326, 19
Mercurio, A., Massarotti, M., Merluzzi, P., Girardi, M., La Barbera, F., & Busarello, G. 2003, A&A, 408, 57
Mo, H. J., Yang, X., van den Bosch, F. C., & Jing, Y. P. 2004, MNRAS, 349, 205
Norberg, P., et al. 2002, MNRAS, 336, 907
Press, W. J., & Schechter, P. 1974, ApJ, 187, 425
Schechter, P. 1976, ApJ, 203, 297
Schmidt, M. 1968, ApJ, 151, 393
Stoughton, C., et al. 2002, AJ, 123, 485
Trentham, N. 1998, MNRAS, 294, 193
Tully, R. B., Somerville, R. S., Trentham, N., & Verheijen, M. A. W. 2002, ApJ, 569, 573
Valotto, C. A., Nicotra, M. A., Muriel, H., & Lambas, D. G. 1997, ApJ, 479, 90
Wolf, C., Meisenheimer, K., Rix, H.-W., Broch, A., Dye, S., & Kleinheinrich, M. 2003, A&A, 401, 73
Xia, L., et al. 2002, PASP, 114, 1349
York, D., et al. 2000, AJ, 120, 1579
Yuan, Q., Zhou, X., & Jiang, Z. 2003, ApJS, 149, 53
Zhou, X., Jiang, Z.-J., Xue, S.-J., Wu, H., Ma, J., & Chen, J.-S. 2001, Chinese J. Astron. Astrophys., 1, 372